Exp. Theo. NANOTECHNOLOGY 10 (2026) 315-328 https://doi.org/10.56053/10.S.315

Green synthesis of CaO from eggshell waste and its impact on SiO_2–Al_2O_3–B_2O_3 –NaF glass-ceramics nanostructure

Kwakeb essam al-hadithy[*], *Dunia k. mahdi*

Department of Physics, College of Science, University of Baghdad, Baghdad, Iraq
[*]) Email: kawakeb.isam1204a@sc.uobaghdad.edu.iq

Received 17/11/2025, *Received in revised form* 15/12/2025, *Accepted* 28/12/2025, *Published* 15/2/2026

White eggshells are used as a natural precursor for the synthesis of calcium oxide (CaO NPs). A series of glass ceramic composite materials are then prepared by combining silicon dioxide (SiO_2), aluminum oxide (Al_2O_3), boron oxide (B_2O_3), sodium fluoride (NaF), and calcium oxide (CaO) derived from eggshells. X-ray diffraction (XRD), Scanning electron microscopy (SEM), Fourier transform infrared spectroscopy (FTIR) are used to understand its effect. XRD analysis confirmed the successful synthesis of CaO NPs from eggshells with high purity. The XRD pattern showed peaks in the produced composite, which corresponds well with those of Si and also presence of quartz (SiO_2). SEM image of composite samples reveals consistent spherical particle morphologies with size (30 to 60 nm). The FTIR spectra further verified the formation of CaO NPs also confirms the presence of compounds that used in synthesized composite. Peaks between 500-400 cm^{-1} indicates the existence of metal oxygen connections. Calcium oxide synthesis from eggshells and its effect on the structure of silicate glass ceramic composite properties.

Keywords: Eggshells; CaO NPs; Glass-ceramic nanostructure.

1. INTRODUCTION

In many industrial industries and in everyday life, glasses are regarded as vital materials [1]. Since glass is recognized as a non-crystalline amorphous solid, it lacks a long-range order of molecular placement and exhibits glass transition behavior in some regions. Glass-ceramics are materials that are first created as glasses (perhaps using glass molding processes) and then heated to improve their characteristics to become ceramics. In general terms, a ceramic is an inorganic, non-metallic solid composed of either metal or non-metal compounds that have been molded and heated to high temperatures to solidify them. Ceramics, as opposed to glass, can have partially or completely

crystalline structures [2,3]. Certain ceramics and glass-ceramics have found widespread use in biomedical applications. Examples include Bioglass®, A–W glass-ceramic, and hydroxyapatite, all of which are well known for their ability to bond with living bone through the formation of a bioactive apatite layer on their surfaces [4]. Glass-ceramic is one of these biomaterials that is particularly helpful due to its superior mechanical qualities and potent bone-bonding capacity [5,6]. It is appealing for orthopedic and dental applications since it is chemically stable and difficult to dissolve in physiological fluids [7].

In parallel with the search for advanced biomaterials, sustainable material sourcing has become increasingly important. Eggshell waste, a byproduct of the food industry, contributes to environmental degradation if not properly managed [8]. Eggshell's primary component is $CaCO_3$, which has several industrial uses. Additionally, $CaCO_3$ is easily transformed into CaO for usage in a variety of applications. [9]. Furthermore, eggshells contain calcium and may be utilized to make other calcium salts instead of calcium carbonate. Similar to CaO, eggshells may be used to create a wide range of additional beneficial materials, such as hydroxyapatite and calcium phosphate bioceramics, which can be implanted as components for various uses [10]. Therefore, if we use environmentally friendly methods to turn eggshells into CaO nanoparticles rather than throwing them away as garbage [11]. They may be effectively employed for a number of uses, including farming. In addition to contributing to environmental cleanliness, using eggshells to produce CaO yields a very effective substance with a wide range of uses, such photocatalytic dye removal [12], biodiesel catalysis[13], heavy metal adsorption[14].

Calcium carbonate itself is found in a variety of natural sources such as limestone, marble, chalk, and marine organisms. It exists in several polymorphic forms including calcite, aragonite, and vaterite, and is considered a primary precursor for CaO, which is also a natural component of human bone [15,16]. For their numerous uses in the industrial, electrical, and agricultural domains, $CaCO_3$ nanoparticles with the appropriate sizes, forms, and morphologies have been the subject of intensive research. [17]. In this study, CaO is prepared from eggshells via thermal decomposition and incorporated into four different glass-ceramic composites composed of SiO_2, Al_2O_3, B_2O_3 and NaF in varying proportions. The structural and morphological characteristics of these composites are analyzed using X-ray diffraction, Scanning electron microscopy and Fourier-transform infrared spectroscopy.

2. MATERIAL AND METHOD

2.1 Synthesis of calcium oxide (CaO) from eggshells

White eggshells are used as a natural precursor for the synthesis of calcium oxide (CaO). Initially, the shells are thoroughly washed with distilled water to remove any adhering impurities and internal organic residues, including proteins. The cleaned shells are then boiled in water for 15 minutes to ensure complete removal of organic content. After boiling, the shells are dried in an oven at 125°C for 15 minutes. Following the drying process, the eggshells are converted into a fine nanostructured powder using electrical mixer, indicating the formation of CaO powder .x-ray are applied to ensure the required oxide.

2.2 Synthesis of glass ceramic composite

A series of composite materials are synthesized by combining silicon dioxide (SiO_2), aluminum oxide (Al_2O_3), boron oxide (B_2O_3), sodium fluoride (NaF), and calcium oxide (CaO) derived from eggshells. The materials are mixed in varying concentrations and subjected to a thermal treatment at 950 °C to promote the formation of homogenous composites. The concentration of SiO_2 is maintained at 5.5 wt% across all four samples. The Al_2O_3 content is varied as follows: 0 wt%, 0.5 wt% and 1wt%, respectively. B_2O_3 is kept constant at 1.5 wt% in all samples, while NaF is fixed at 2 wt%. The CaO

content, sourced from calcined eggshells, is altered across the samples with values of 0 wt%, 0.5 wt%, and 1 wt% respectively. This compositional variation is designed to investigate the influence of CaO and Al_2O_3 content on the structural and thermal behavior of the resulting composites.

2.3 Characterization

The structure of the CaO nanoparticles glass ceramic composite is examined by X-ray diffraction (Philips PW1730) with Cu-Kα radiation source (λ = 0.154 nm) at 2θ = 20◦–90◦. Fourier transform infrared (FTIR) Spectroscopy measurement (sgimadzu 1800) is used to measure the composition and chemical bonds by measuring the absorption or emission of the infrared spectrum. Field emission scanning electron microscopy (FE-SEM) (Tescan MIRA III), which operates at (20–30 KV) and (8000–60000 X) magnifications to observe morphology.

3. RESULTS AND DISCUSSION

3.1 XRD of CaO NPs

The XRD pattern of the prepared calcium oxide NPs is shown in Figure (1). The typical reflection from the (111), (020), (022), (040), (131), (222), (040) and (133) planes is seen in the produced, which corresponds well with those of CaO that are found from JCPDS card no. 96-900-6713. These findings align with those reported in earlier studies[18,19] The product's high purity is confirmed by the absence of additional impurity peaks in the XRD spectra[20,21] The crystallite sizes for the product are determined using the Debye–Scherrer formula based on the highest intensity (020) peak, and the results are presented in Table 1.

$$\mathrm{D} = \frac{k\lambda}{\beta \cos\theta} \quad (1)$$

where k = shape factor, λ = 1.54060Å, β = Full Width Half Maximum (FWHM) and θ = diffracting angle. The found crystallite size is 79 nm this indicated that prepared CaO specimen are nanocrystalline powder. While previous study [22] derived CaO from oyster shells at pH 10 is found the crystallite size approximately 89.5 nm. The x-ray approved that the CaO-NPs has a cubic crystal, therefore, lattice parameters for each set of Miller indices are calculated using the following equation[23]

$$a = d_{spacing} * \sqrt{h^2 + k^2 + l^2} \quad (2)$$

where, (h k l) are plane indices for the peak in the XRD pattern, $d_{spacing}$ interplanar spacing and a is the lattice parameter. The calculated lattice parameters are shown in Table (1), which is identical to the expected value for the reference CaO from JCPDS card no. 96-900-6713. This observation indicated successful phase formation and high structural purity [24].

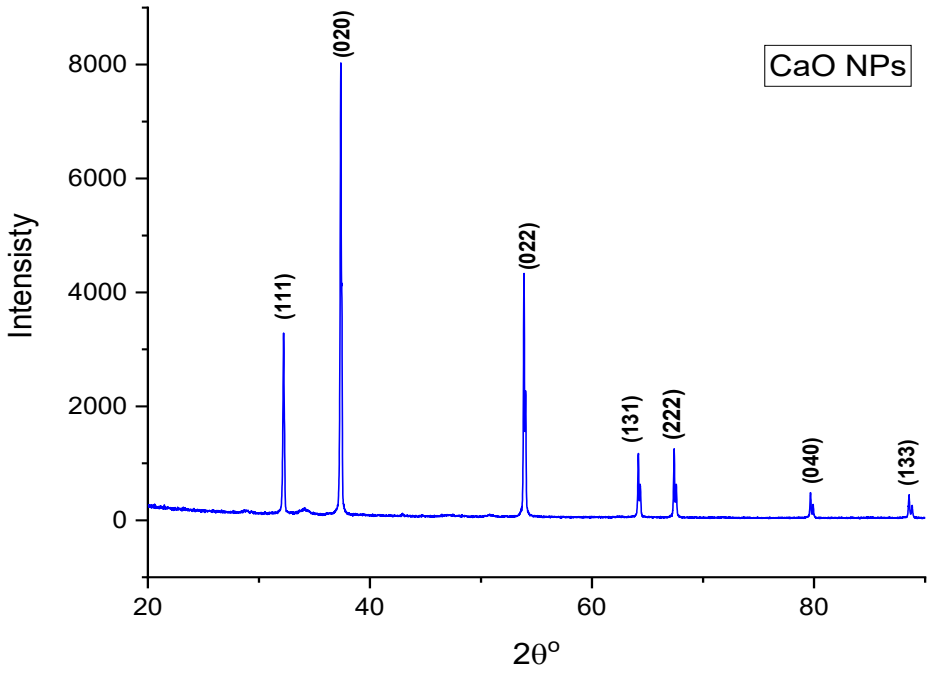

Figure 1 XRD for CaO nanoparticles.

Table 1 Calculated lattice parameters of CaO.

Sample	2θ (degree)	FWHM (degree)	D (nm)	D spacing	Lattice Constant (a) Å
CaO	37.3554	0.1106	79.19	2.40535	4.810
JCPDS	37.353			2.40550	4.810

3.2 XRD of glass ceramic composite

The XRD pattern of the prepared composite with various content ratios is shown in Figure (2). The typical reflection from the (111), (022), (131), (040), (422), (133), and (242) planes is seen in the produced composite, which corresponds well with those of Si that found from JCPDS card no. 96-151-2542. The XRD result indicated the presence of quartz (SiO_2) at 2θ = 26.45° according to JPCDS card no. 46-1045 as the dominant crystalline phase across all samples with additional peaks corresponding to secondary phases. These findings are in line with previous studies [25,26]. Peaks at 21.87° and 38.73° are related to Mullite ($3Al_2O_3{\cdot}2SiO_2$) according to JPCDS card no.15-0776. The formation of Mullite is expected to be enhanced at temperatures above 1000°C. Research suggests that fluoride compounds can significantly reduce the mullite formation temperature in ($Al_2O_3{\cdot}SiO_2$) systems [27]. There are no peaks related to CaO, B_2O_3, and NaF. This can be due to the fact that the CaO may have reacted with SiO_2 to form calcium silicates (e.g., wollastonite or an amorphous calcium silicate phase), which may not be detectable in XRD due to low crystallinity or overlapping peaks [28]. B_2O_3 can form borosilicate or borate phases, which are often poorly crystalline and difficult to detect using conventional XRD [29]. NaF might be incorporated into the silica network or volatilized at high temperatures, reducing its presence as a distinct phase [30]. Al_2O_3 is known to influence the crystallization process and can help form well-defined, high-intensity diffraction peaks. Its absence may have led to the dominance of an amorphous or poorly crystallized phase, resulting in lower peak

intensity in the S3[31]. Also, the reduced intensity of peaks in S3 can be attributed to the formation of amorphous phases influenced by the presence of CaO. Research indicates that CaO can promote amorphous phase separation in glass systems, leading to decreased crystallinity and consequently lower peak intensities[32]. The crystallite sizes for all glass ceramic composite samples are determined using eq (1), and the results are presented in Table 2.

From the table, it is clear that there is a change in crystal size. The variation in crystallite size across samples, influenced by differing Al_2O_3 and CaO contents, align with findings in existing previous studies. Mukherjee et al [33] study of SiO_2–Al_2O_3–CaO glass-ceramics, it has been indicating an influence changing the Al_2O_3 content at the expense of SiO_2 upon crystallization mechanism and microstructure and therefore upon crystallite size. Keyvani et al [34] investigate the influence of Al_2O_3 content upon the crystallization characteristics, of SiO_2-Al_2O_3-CaO-MgO glass-ceramics, the experimental search has found that the increasing of Al_2O_3 content at the expense of SiO_2 has a significant impact on the nucleation and crystallization mechanism, and also changes the crystallite size. Shi et al [35] also found that CaO content affected on the crystallite size, increasing CaO content generally promotes crystallization.

Table 2 Crystallite size of all samples.

Sample	SiO_2 (wt%)	Al_2O_3 (wt%)	B_2O_3 (wt%)	NaF (wt%)	CaO (wt%)	2θ (degree)	FWHM (degree)	D (nm)
S 1	5.5	1	1.5	2	0	28.23	0.140	60.94
S 2	5.5	0.5	1.5	2	0.5	28.38	0.167	51.03
S 3	5.5	0	1.5	2	1	28.24	0.515	16.61
S 4	5.5	0.5	1.5	2	1	28.13	0.163	52.48

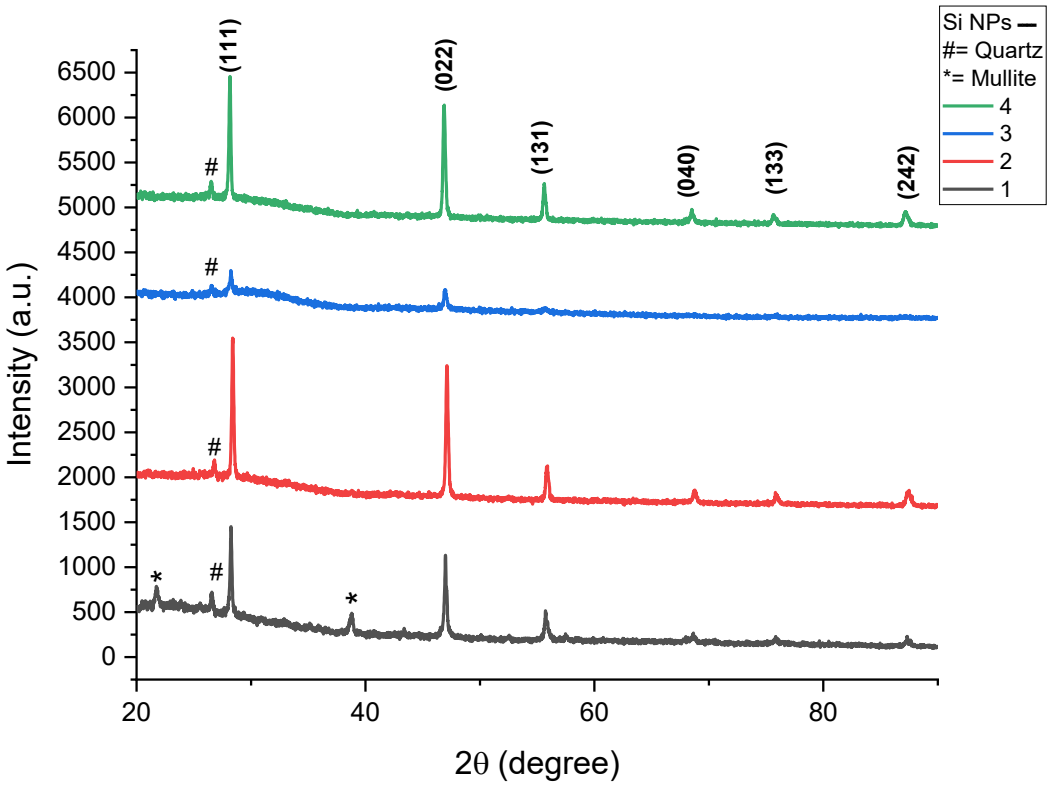

Figure 2 XRD of all prepared silicate glass samples.

3.3 FTIR of CaO NPs

The FTIR spectrum Figure (3) of the extracted CaO NPs depicts a certain vibrational band which confirmed successful formation of CaO and existence of some surface-bound species. A fairly broad peak around 3436 cm^{-1} is assigned to O-H stretch vibration from surface-adsorbed moisture or hydroxyl groups[36]. The creation of pure phase particles is indicated by this peak's acute well[37]. The shallow depth of this bond indicates that the prepared and tempering process is proper. Bands at 2853 and 2923 cm^{-1}, is attributed to the C–H stretching vibrations[38]. CaO exhibits spectra at 471, 579 and 1742 cm^{-1} that are corresponding to the presence of CaO[24,39]. Some researchers explain that the bending vibration at 1631 cm^{-1} is due to H–O–H water adsorbed molecules[40]. The carbonation of CaO to CaO-NPs is shown by the band at 1465 cm^{-1}, which is also linked to C-O absorption[23]. The peak observed at 1070 cm^{-1} and 795 cm^{-1} is also typical for CaO [23,41]. The FTIR spectra bands of CaO NPs are shown in Table 3.

Table 3 FTIR spectra bands of CaO NPs.

Peak	Assignment
3436.88	O-H stretch vibration
2923.70 2853.14	C–H stretching vibrations
1631.35	H–O–H bending vibration
1465.46	C-O stretching vibrations
1742.39 1070.89 795.30 579.91 471.56	Ca–O lattice vibration

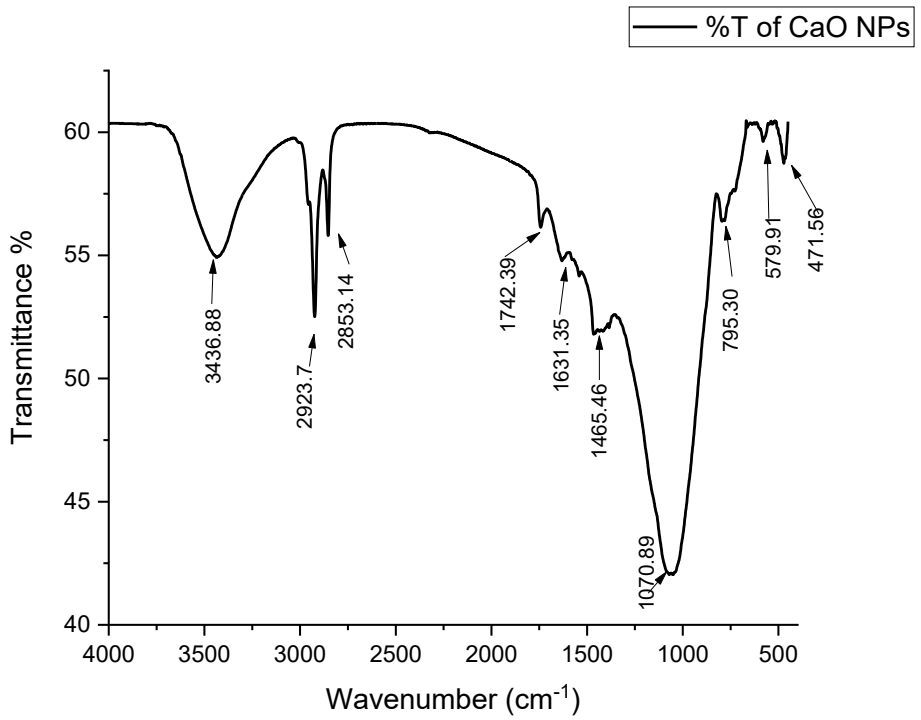

Figure 3 FTIR spectrum of extracted CaO NPs.

3.4 FTIR of glass ceramic composite

The FTIR spectra of the four samples in figure (4) show specific vibrational bands attributable to their constituents, reflecting changes in molecular bonding caused by differences in composition. A peak characteristic of O–H stretching can be seen prominently in the spectra of S1 at 3462 cm^{-1} and at 3412 cm^{-1}, suggesting that some hydroxyl groups are formed via adsorption of moisture onto the surface[42-44]. The same trend is noted for Samples 2, 3, and 4, only displaced to 3545 cm^{-1} (S2, S3) and 3539 cm^{-1} (S4); an indication of minimal differences in the strength of hydrogen bonding[45]. The peaks at 2852-3008 cm^{-1} in the S1 represented the C-H stretching modes that shifted to the region of 2924-3003 cm^{-1} in S3, signifying some changes in the organic residuals or maybe modification of structures due to increasing amount of CaO[46,47]. The stretching bands of B-O revealing are found at 1085 cm^{-1} (S1) and 1618 cm^{-1} (S2, S3, S4), which confirms the presence of compounds that contain boron[48].

Absorption bands around 1745 cm^{-1} and 1616 cm^{-1} are typically due to the carbonyl (C=O) stretching vibrations and stretching vibrations of aromatic C=C bonds, respectively [42].

The presence of these peaks suggested interactions between the Al_2O_3 and CaO phases, which ultimately lead to the formation of carbonate species. Such interactions are likely to alter the vibrational modes of the composite material[49]. S2,S3, and S4 exhibit shifting peaks at 796 cm^{-1}, 634 cm^{-1}, and 576 cm^{-1} from their original positions as found in S 1, which are associated with the bending vibrations from Si–O–Si and Al–O bonds[49,50].peaks between 500-400 cm^{-1} indicates the existence of metal oxygen connections[51]. In a related context Fan *et al* [52]in 2022 found when the amount of CaO in the glass ceramic increases, the free oxygen that CaO introduces encourages the conversion of $[AlO_6]$ into $[AlO_4]$, which causes the Si–O–Al bond between $[SiO_4]$ and $[AlO_4]$ to gradually increase. As a result, both of them move from a low wave number segment to a high wave number segment, and the vibration peak intensity near 715 cm^{-1} is gradually enhanced. The FTIR spectra bands of the four Composite samples are shown in Table 4.

Table 4 FTIR spectra of the prepared silicate glasses.

S1	S2	S3	S 4	Bond
3462	3545 3468	3545 3475	3539 3464	O–H stretching (hydroxyl)
3412	3410	3412	3412	H-bonded O-H
3242 3008 2924 2852	3240 3008 2924 2852	3240 3003 2922 2852	3232 2922 2852	C-H stretching
1745	1745	1745	1743	carbonyl (C=O) stretching vibrations
1616	1635 1618	1635	1635 1616	stretching vibrations of aromatic C=C bonds
			1552	O–H bending
1448	1413	1448	1462	asymmetric stretching of CO32
1085	1047	1056 950	1132 1060	Si-O stretching
796 634 576	796 607	736 638 536	831 785 702 640 613 553 520	vibrations from Si–O–Si and Al–O bonds
447	455	466 414	460 426	Metal-oxygen bond

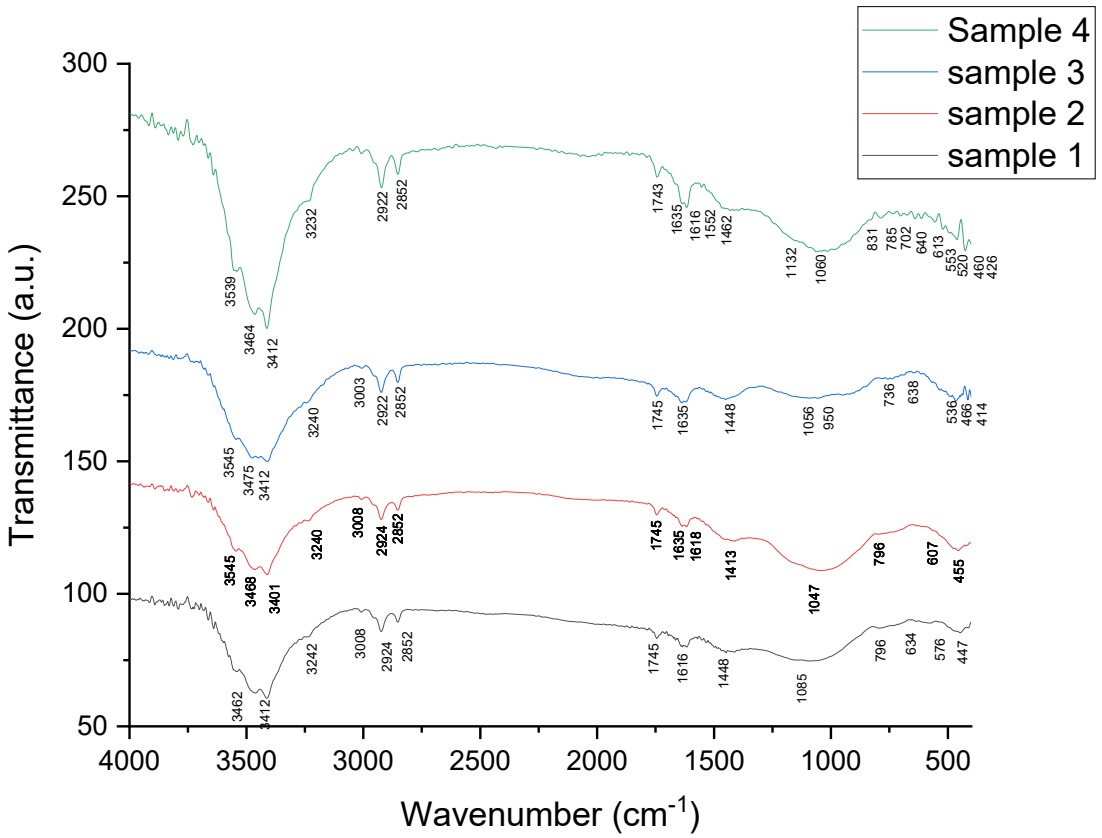

Figure 4 FTIR spectra of the four Composite samples.

3.5 SEM of glass ceramic composite

SEM analysis of all composite samples is shown in figure 5 to figure 8, reveals consistent spherical particle morphologies across the materials indicating controlled nucleation and growth processes during synthesis. The particle sizes vary systematically, where sample with composition S1 exhibits larger particles approximately (40 nm to 60 nm) while samples S2, S3 and S4 show smaller and more uniform particle sizes ranging from approximately (30 nm to 50 nm). The decrease in Al_2O_3 content and increase in CaO content in S2, S3, and S4 leads to a trend towards finer particle formation and improved dispersion, this result are shown in [53]. Surface textures are generally smooth, indicating high crystallinity but exhibit some roughness area probably due to differences in phase composition or secondary phase [54]. Good particle dispersion with minimal agglomeration is exhibited in all samples, demonstrating suitable processing conditions that may involve the use of stabilizers or surfactants. These observations obtained using the SEM are consistent with synthetic trends of XRD data, providing a comprehensive understanding of how differences in chemical composition affect the exact properties of the structure. While previous research showed the NPs stuck together, which may be due to the drying of the sample before being analyzed by SEM[55]. However, Kozlovskiy *et al.* [56] found that when the concentration of oxide dopants increases in the glass ceramic composite, the number of these grains increases along with their size, and agglomeration inclusions develop in the composition. The production of impurity phases may be the cause of these structures, and the way these grains are arranged suggests that structures in the form of an interstitial or substitutional solid solution have formed.

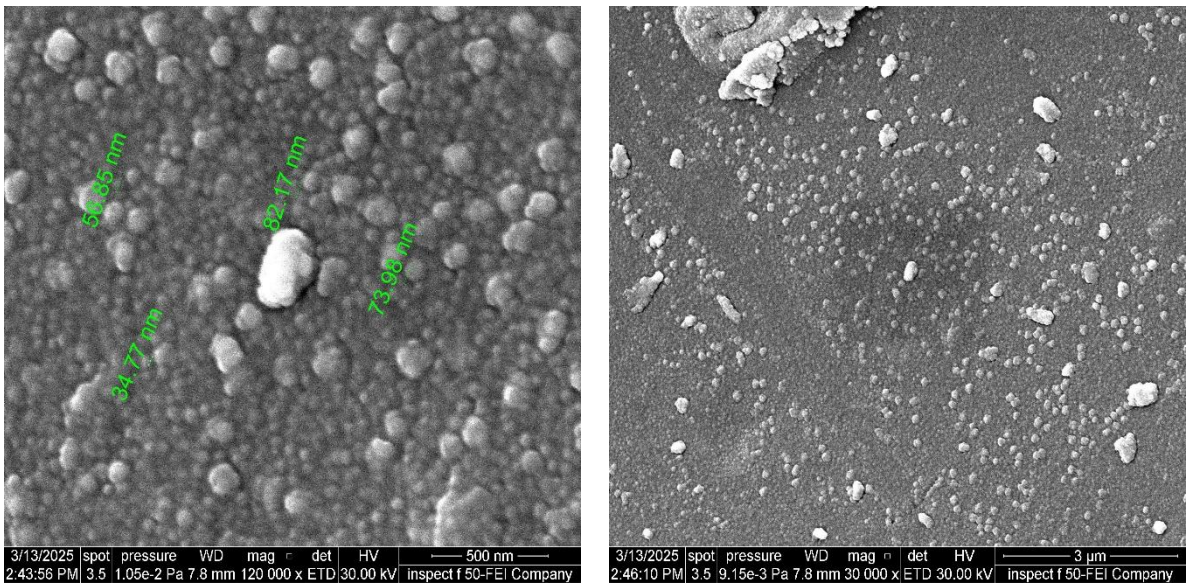

Figure 5 SEM of sample S1.

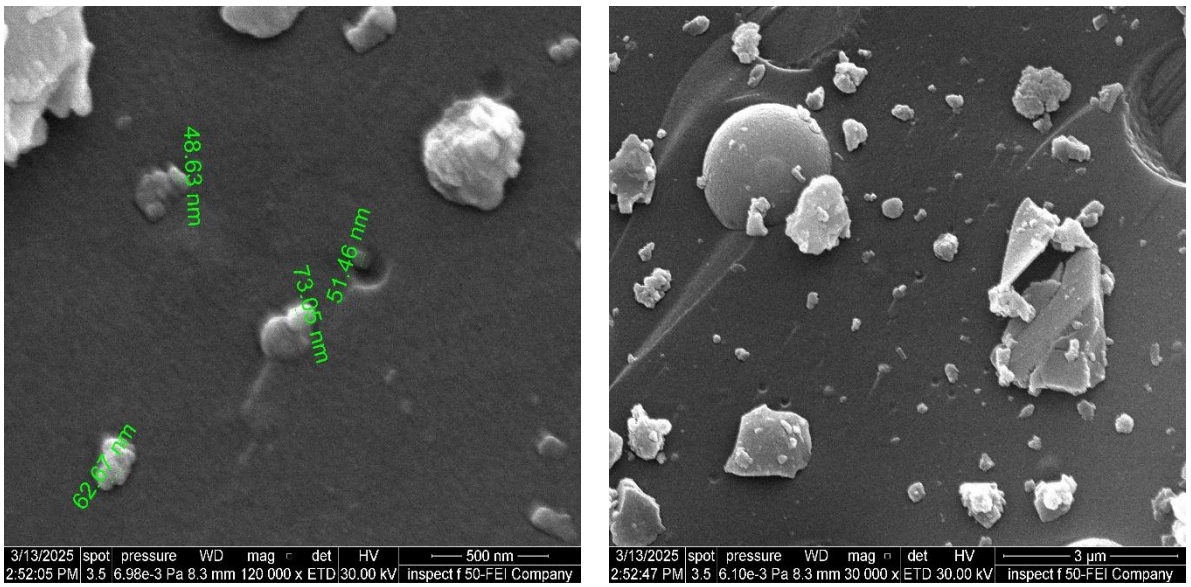

Figure 6 SEM of sample S2.

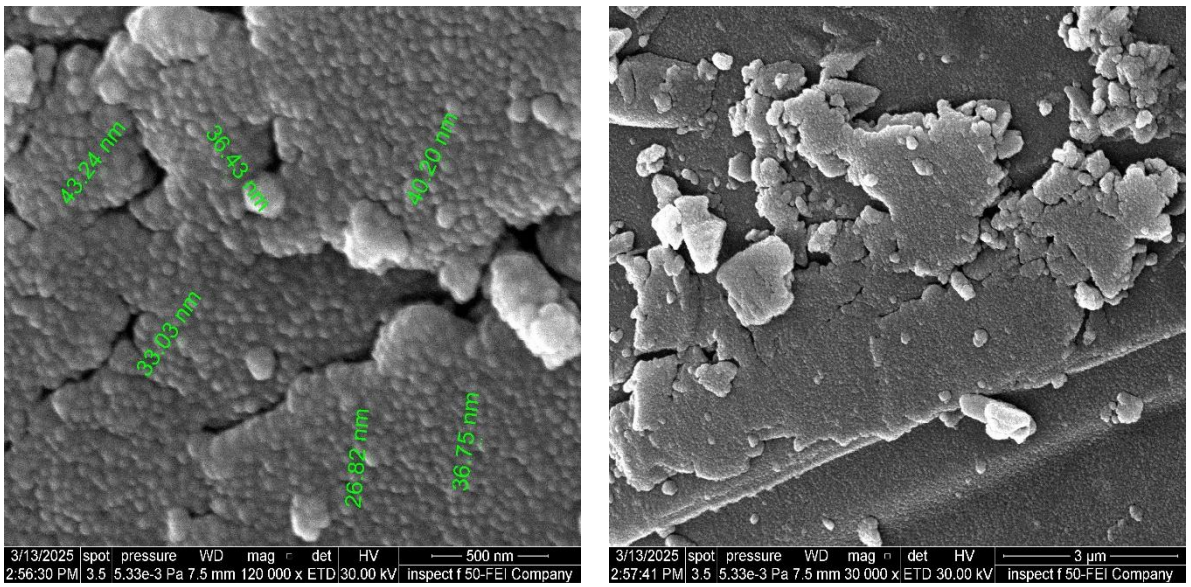

Figure 7 SEM of sample S3.

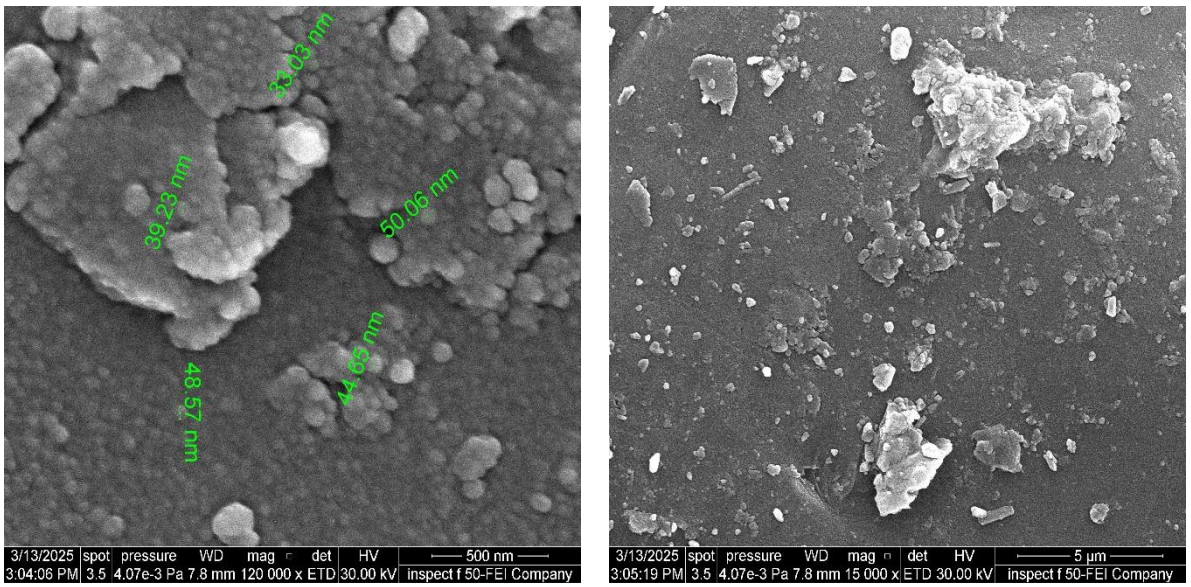

Figure 8 SEM of sample S4.

4. CONCLUSIONS

This work showed that calcium oxide nanoparticles can be prepared successfully from eggshells, with an average crystallite size around 79 nm. When mixed with SiO_2, Al_2O_3, B_2O_3 and NaF to form glass–ceramic composites, the XRD patterns mainly revealed quartz, and in some cases weak peaks that could be related to mullite. It was noticed that changing the amount of CaO and Al_2O_3 affected the crystallite size, where sample S3 gave the smallest value and seemed to be more amorphous. The SEM images confirmed that the glass ceramic composite particles are mostly spherical with sizes between 30–60 nm, and higher CaO content seemed to produce finer particles. FTIR spectra also showed the main bonds of Si–O, Al–O, B–O and Ca–O. These results suggest that waste eggshells can be a useful and cheap source of CaO for making glass–ceramic composites.

References

[1] B.A.E. Ben-Arfa, I.M. Miranda Salvado, J.M.F. Ferreira, R.C. Pullar, Int. J. Appl. Glas Sci. 8 (2017) 337 https://doi.org/10.1016/j.msec.2018.05.016
[2] M.S.K. Mubina, S. Shailajha, R. Sankaranarayanan, L. Saranya, J. Mech. Behav. Biomed. Mater. 100 (2019) 103379 https://doi.org/10.1016/j.jmbbm.2019.103379
[3] R.H. Hassan, D.K. Mahdi, Iraqi J. Phys. 22 (2024) 104 https://doi.org/10.30723/tfm9wa89
[4] M. Riaz, R. Zia, F. Saleemi, H. Ikram, F. Bashir, J. Mater. Sci. Mater. Med. 26 (2015) 1 https://doi.org/10.1007/s10856-015-5603-3
[5] H. Fujita, H. Iida, K. Ido, Y. Matsuda, M. Oka, T. Nakamura, J. Bone Joint Surg. Br. 82 (2000) 614 https://doi.org/10.1302/0301-620X.82B4.0820614
[6] T.A. Kareem, D.K. Mahdi, Eurasian Chem. Commun. 4 (2022) 330 https://doi.org/10.22034/ecc.2022.326506.1311
[7] S.M. Salman, S.N. Salama, H. Darwish, H.A. Abo-Mosallam, Ceram. Int. 35 (2009) 1083 https://doi.org/10.1016/j.ceramint.2008.04.025
[8] K. Adaikalam, A.M. Teli, K.P. Marimuthu, S. Ramesh, H. Lee, H.S. Kim, et al., Nanomaterials 14 (2024) 1129 https://doi.org/10.3390/nano14131129
[9] M.Y. Chou, T.A. Lee, Y.S. Lin, S.Y. Hsu, M.F. Wang, P.H. Li, et al., Sci. Rep. 13 (2023) 437 https://doi.org/10.1038/s41598-023-27682-5
[10] Y.C. Wong, R.X. Ang, Open Chem. 16 (2018) 1166 https://doi.org/10.1515/chem-2018-0127
[11] A. Anantharaman, S. Ramalakshmi, M. George, Int. J. Eng. Res. Appl. 6 (2016) 27 https://doi.org/10.1038/s41598-022-06981-3
[12] K. Adaikalam, S. Hussain, P. Anbu, A. Rajaram, I. Sivanesan, H.S. Kim, Nanomaterials 14 (2024) 1620 https://doi.org/10.3390/nano14201620
[13] J.A. Tavizón-Pozos, H. Cervantes-Cuevas, G.G. Garcia-Camacho, G. Chavez-Esquivel, D.R. Acosta-Najarro, ACS Omega 10 (2025) 6827 https://doi.org/10.1021/acsomega.4c09118
[14] T.A.E. Ahmed, L. Wu, M. Younes, M. Hincke, Front. Bioeng. Biotechnol. 9 (2021) 675364 https://doi.org/10.3389/fbioe.2021.675364
[15] A.Z. Jaji, M.Z.B.A. Bakar, R. Mahmud, M.Y. Loqman, M.N.M. Hezmee, T. Isa, et al., Nanotechnol. Sci. Appl. 10 (2017) 23 https://doi.org/10.2147/NSA.S113030
[16] S. Maleki, M. Barzegar-Jalali, M.H. Zarrintan, K. Adibkia, F. Lotfipour, Pharm. Sci. 20 (2015) 175 https://doi.org/10.1038/s41598-020-75454-2
[17] O.V. Kharissova, H.V.R. Dias, B.I. Kharisov, B.O. Pérez, V.M.J. Pérez, Trends Biotechnol. 31 (2013) 240 https://doi.org/10.1016/j.tibtech.2013.01.003
[18] R. Mohadi, A. Sueb, K. Anggraini, A. Lesbani, J. Pure Appl. Chem. Res. 7 (2018) 130 https://doi.org/10.21776/ub.jpacr.2018.007.02.390
[19] V. Bhuvaneshwari, S. Sonia, D. Sivaganesh, Chem. Phys. Impact 9 (2024) 100699 https://doi.org/10.1016/j.chphi.2024.100699
[20] N. Ojha, I. Dmitrieva, W. Blanc, L. Petit, Ceramics 4 (2021) 148 https://doi.org/10.3390/ceramics4020013
[21] Z. Zhang, H. Ma, C. Wu, Y. Sun, R. Chen, X. Guo, Separations 10 (2023) 498 https://doi.org/10.3390/separations10090498
[22] S. Rujitanapanich, P. Kumpapan, P. Wanjanoi, Energy Procedia 56 (2014) 112 https://doi.org/10.1016/j.egypro.2014.07.138
[23] N.O. Eddy, J. Oladede, I.S. Eze, R. Garg, R. Garg, H. Paktin, Results Eng. 24 (2024) 103374 https://doi.org/10.1016/j.rineng.2024.103374
[24] A. Roy, J. Bhattacharya, Nanotechnol. 3 (2011) 565 https://doi.org/10.1016/j.rio.2024.100677
[25] A.M. Elbarbary, M.A. Elhady, Y.H. Gad, J. Inorg. Organomet. Polym. Mater. 32 (2022) 4039 https://doi.org/10.1007/s10904-022-02395-w

[26] Y. Lu, Y. Shan, X. Guo, Y. Zhang, J. Feng, H. Zhou, J. Mater. Sci. Mater. Electron. 34 (2023) 443 https://doi.org/10.1007/s10854-023-09902-w
[27] J. Li, Y. Wu, Y. Pan, W. Liu, J. Guo, Ceram. Int. 33 (2007) 919 https://doi.org/10.1016/j.ceramint.2006.02.002
[28] N. Yamaguchi, Y. Masuda, Y. Yamada, H. Narusawa, H.-C. Han, Y. Tamaki, et al., Open J. Inorg. Non-Metallic Mater. 5 (2014) 1 https://doi.org/10.2298/PAC2202115T
[29] A. Behairy, New J. Glas Ceram. 9 (2019) 15 https://doi.org/10.1007/s13369-024-08988-6
[30] A. Abd El-Moneim, H.A. Hashem, A.A. El-Namrouty, A. Atef, J. Non-Cryst. Solids 580 (2022) 121389 https://doi.org/10.1016/j.jnoncrysol.2021.121389
[31] W. Zheng, J.M. Wu, S. Chen, C.S. Wang, C.L. Liu, S.B. Hua, et al., J. Adv. Ceram. 10 (2021) 1381 https://doi.org/10.1007/s40145-021-0513-y
[32] J.M. Oliveira, R.N. Correia, M.H. Fernandes, J. Non-Cryst. Solids 273 (2000) 59 https://doi.org/10.1016/S0022-3093(00)00144-7
[33] D.P. Mukherjee, S.K. Das, Ceram. Int. 39 (2013) 571 https://doi.org/10.1016/j.ceramint.2012.06.066
[34] M. M. Abbas, M. Rasheed, J. Phys. Conf. Ser., 1795(1) (2021) 012059 https://doi.org/10.1088/1742-6596/1795/1/012059.
[35] P.Y. Shi, M.F. Jiang, C.J. Liu, D.Y. Wang, J. Northeast Univ. (Nat. Sci.) 25 (2004) 866 https://doi.org/10.1044/jshd.2404.330
[36] A. Khan, S.T. Hussain, A. Naeem, A. Sadiqa, A. Ahmad, M.A.A. Shehzada, et al., Results Chem. 12 (2025) 102073 https://doi.org/10.3390/catal15100970
[37] M. Rasheed, SuhaShihab, O. Alabdali, H. H. Hassan, J. Phys. Conf. Ser., 1879(3) (2021) 032113 https://doi.org/10.1088/1742-6596/1879/3/032113.
[38] D. MEKAM, D. MESRI , H. Rozale. Experimental and Theoretical NANOTECHNOLOGY, 3(3) (2019) 281 https://doi.org/10.56053/3.3.281.
[39] I. Fatimah, G.R. Aulia, W. Puspitasari, R. Nurillahi, L. Sopia, R. Herianto, Sustain. Environ. Res. 28 (2018) 462 https://doi.org/10.1016/j.serj.2018.10.003
[40] A.J. Hussein, M.N. Al-Darraji, M. Rasheed, M.A. Sarhan, IOP Conf. Ser.: Earth Environ. Sci. 1262 (2023) 022005 https://doi.org/10.1088/1755-1315/1262/2/022005.
[41] A.I. Hussein, Z. Ab-Ghani, A.N. Che Mat, N.A. Ab Ghani, A. Husein, I. Ab. Rahman, Appl. Sci. 10 (2020) 7170 https://doi.org/10.3390/app10207170
[42] T. Saidani, M. Rasheed, I. Alshalal, A.A. Rashed, M.A. Sarhan, R. Barillé, Res. Eng. Struct. Mater. 10 (2) (2024) 743 http://dx.doi.org/10.17515/resm2023.21ma0922rs.
[43] F. Dai, Q. Zhuang, G. Huang, H. Deng, X. Zhang, ACS Omega 8 (2023) 17064 https://doi.org/10.1021/acsomega.3c01336
[44] M. A. Sarhan, S. Shihab, B. E. Kashem, M. Rasheed, J. Phy.: Conf. Ser., 1879(2) (2021) 022122 https://doi.org/10.1088/1742-6596/1879/2/022122.
[45] I. León, R. Montero, A. Longarte, J.A. Fernández, J. Phys. Chem. Lett. 12 (2021) 1316 https://doi.org/10.1021/acs.jpclett.0c03001
[46] S. Mukherjee, S. Das, S. Nuthi, C.R. Patra, Future Sci. OA 3 (2017) FSO233 https://doi.org/10.4155/fsoa-2017-0048
[47] J. Anastassopoulou, P. Kolovou, P. Papagelopoulos, T. Theophanides, Infrared Spectrosc. Life Biomed. Sci. 25 (2012) 259 https://doi.org/10.1038/s41598-021-86257-4
[48] S. Mondal, A.K. Banthia, J. Eur. Ceram. Soc. 25 (2005) 287 https://doi.org/10.1016/j.jeurceramsoc.2004.08.011
[49] A. M. Shehap, Kh.H. Mahmoud, M.F.H. Abdelkader, Tarek M. El-Basheer, Experimental and Theoretical NANOTECHNOLOGY 1 (2017) 103 https://doi.org/10.56053/1.2.103.
[50] P.A. Bhat, N.C. Debnath, IOP Conf. Ser.: Mater. Sci. Eng. 53 (2013) 012001 https://doi.org/10.1021/acssusresmgt.5c00359

[51] Badis Bendjemil, Mahiedinne Ali-Rachedi, Jamal Bougdira, Faming Zhang, Eberhard Burkel, Experimental and Theoretical NANOTECHNOLOGY 1 (2017) 145 https://doi.org/10.56053/1.3.145.
[52] L.A. Carrero Bermúdez, R. Moreno Mendoza, R. Cardona, D.A. Landínez Téllez, J. Roa-Rojas, Experimental and Theoretical NANOTECHNOLOGY 1 (2017) 161 https://doi.org/10.56053/1.3.161.
[53] Rida Ahmed Ammar, Experimental and Theoretical NANOTECHNOLOGY 2 (2018) 1 https://doi.org/10.56053/2.1.1.
[54] H. Rashid, Eur. J. Dent. 8 (2014) 571 https://doi.org/10.4103/1305-7456.143646
[55] A.M. Abduljabar, N.N. Hussein, Iraqi J. Sci. 64 (2023) 6226 https://doi.org/10.24996/ijs.2023.64.12.12
[56] A.L. Kozlovskiy, D.I. Shlimas, M.V. Zdorovets, E. Elsts, M. Konuhova, A.I. Popov, Materials 16 (2023) 2366 https://doi.org/10.3390/ma16062366